ISSN 1560-3547, Regular and Chaotic Dynamics, 2018, Vol. 23, Nos. 7–8, pp. 803–820. © Pleiades Publishing, Ltd., 2018.

# Comparing Dynamics Initiated by an Attached Oscillating Particle for the Nonholonomic Model of a Chaplygin Sleigh and for a Model with Strong Transverse and Weak Longitudinal Viscous Friction Applied at a Fixed Point on the Body

**Alexey V. Borisov[1, 2*] and Sergey P. Kuznetsov[1, 3**]**

[1] *Udmurt State University, ul. Universitetskaya 1, Izhevsk, 426034 Russia*

[2] *Moscow Institute of Physics and Technology, Institutskii per. 9, Dolgoprudnyi, 141700 Russia*

[3] *Kotel'nikov's Institute of Radio-Engineering and Electronics of RAS, Saratov Branch, ul. Zelenaya 38, Saratov, 410019 Russia*

Received October 30, 2018; accepted November 28, 2018

**Abstract**—This paper addresses the problem of a rigid body moving on a plane (a platform) whose motion is initiated by oscillations of a point mass relative to the body in the presence of the viscous friction force applied at a fixed point of the platform and having in one direction a small (or even zero) value and a large value in the transverse direction. This problem is analogous to that of a Chaplygin sleigh when the nonholonomic constraint prohibiting motions of the fixed point on the platform across the direction prescribed on it is replaced by viscous friction. We present numerical results which confirm correspondence between the phenomenology of complex dynamics of the model with a nonholonomic constraint and a system with viscous friction — phase portraits of attractors, bifurcation diagram, and Lyapunov exponents. In particular, we show the possibility of the platform's motion being accelerated by oscillations of the internal mass, although, in contrast to the nonholonomic model, the effect of acceleration tends to saturation. We also show the possibility of chaotic dynamics related to strange attractors of equations for generalized velocities, which is accompanied by a two-dimensional random walk of the platform in a laboratory reference system. The results obtained may be of interest to applications in the context of the problem of developing robotic mechanisms for motion in a fluid under the action of the motions of internal masses.

MSC2010 numbers: 37C10, 34D45, 37E30, 34C60, 37J60

**DOI:** 10.1134/S1560354718070018

Keywords: Chaplygin sleigh, friction, parametric oscillator, strange attractor, Lyapunov exponents, chaotic dynamics, fish-like robot

## INTRODUCTION

One of the interesting and important problems of robotics is to develop mobile devices, including those moving in the volume or on the surface of a fluid by changing the position of the internal masses [1–3]. Strictly speaking, the description of the dynamics and control of such systems must be based on the solution of equations that include hydrodynamical (Navier – Stokes) equations for a liquid medium. This is a rather complicated problem, which requires considerable computational resources, and control on this basis in the real-time mode can be difficult. In this connection, it would be natural to make use of description methods within the framework of finite-dimensional models [4–9] in cases where such a description can be sufficiently accurate.

* E-mail: borisov@rcd.ru

** E-mail: spkuz@yandex.ru

It appears that it may be rewarding to proceed from the models of mechanical systems with nonholonomic constraints. A good and concrete example is provided by the problem of a Chaplygin sleigh, which deals with the motion of a rigid body, a platform on the plane (or another surface) subject to the nonholonomic constraint prohibiting motions for a fixed point on the platform across the direction prescribed at this point [10–12]. Physically, it can be thought of as the presence of a support secured to the platform in the form of a skate or a knife edge, which prevents transverse motions of the point of contact of the body with the plane. The recent papers [13–20] are devoted to a number of modifications of the classical problem, in particular, to the motion of a Chaplygin sleigh under periodic external action and under periodic changes of the position of the point of application of the nonholonomic constraint. In the situation where the motion of the system is ensured by periodic displacements of the internal mass, the possibility was demonstrated of unbounded acceleration of the directed motion of the system [16–18] which is, in a sense, an analog of the well-known effect of Fermi's acceleration [11–25]. In the case where there is nonzero friction in the direction of the knife edge which ensures the nonholonomic constraint, there is another mechanism of unbounded growth of the kinetic energy of the system due to parametric instability, which takes place under certain conditions in the case of a relatively large amplitude of oscillatory motion of the internal mass, which constitutes an appreciable portion of the total mass of the system [5, 17]. The possibility of chaotic dynamics which involves strange attractors in dynamical equations in the space of generalized velocities is also shown. In this case, motions classified as two-dimensional random walks [16, 17] take place in the laboratory reference system. The presence of the modes of chaotic dynamics enables motion control by correctly selected small variations of the system parameters, as is done within the framework of the area known as chaos control [26].

There are some well-known studies where the possibility of replacing the nonholonomic constraint by viscous friction [27–30] is established. In the case of a Chaplygin sleigh this implies that motions across the knife edge are not completely prohibited, but are characterized by a large friction coefficient. If one restricts oneself to models where the friction force is applied at a fixed point of the platform, then the above-mentioned results concerning the Chaplygin sleigh can serve as a natural starting point for analysis of dynamical phenomena. For bodies moving in a fluid or on the surface of a fluid, such models can be regarded as an approximate description of situations where the body has a keel that ensures strong viscous friction across its direction and weak friction in the longitudinal direction, under the assumption that the dimensions of the keel are smaller than those of the platform[1)].

The goal of this paper is to compare the dynamical phenomena caused by oscillatory motions of the internal mass, for the nonholonomic model of a Chaplygin sleigh and for the model where the action of the medium on the motion of the platform is determined by the friction force applied at the fixed point, by replacing the effect of a nonholonomic constraint.

Section 1 formulates the basic equations and discusses the question as to how they are related to the equations of the nonholonomic model of a Chaplygin sleigh. Section 2 deals with the effect of acceleration of the motion of the platform under small oscillations of the internal mass. It is shown that this effect persists when the nonholonomic constraint is replaced by transverse viscous friction in the region of small velocities, but, in contrast to the nonholonomic model, the increase in the velocity has the tendency to saturation. Section 3 discusses the question as to how two types of chaotic attractors occurring in the space of generalized momenta of the nonholonomic model are transformed in the system with friction: fractal attractors, similar to those in dissipative systems [33–35], and "fat" attractors, similar to the "chaotic sea" in Hamiltonian systems [35–37]. It is shown that, apart from some minor changes, the attractors of the first type persist when the nonholonomic constraint is replaced by viscous friction, and the attractors of the second type break down, resulting in the formation of many coexisting regular attractors in the form of attracting cycles. Section 4 analyzes and compares, for the nonholonomic model and for systems with friction, the dynamical regimes associated with strange attractors, which in the laboratory reference system correspond to motions in the form of two-dimensional random walks [38–40]. It is shown that in the system with viscous friction these motions are characterized by a smaller value of the diffusion coefficient than those in the nonholonomic model. Section 5 is concerned with

[1)] It is appropriate at this point to mention the well-known classical result in hydrodynamics — the generalization of the Stokes formula to the case where a body moving in a viscous fluid has the shape of an ellipsoid; in this case, the drag coefficients are different for motions in the direction of different axes of the ellipsoid [31].

the effect of parametric resonance [41–43], which in the nonholonomic model, where longitudinal viscous friction is taken into account, can lead to an unbounded growth of the kinetic energy of the platform during unbounded excitation of the oscillation amplitude [17, 18]. It is shown that a system where the nonholonomic constraint is replaced by transverse viscous friction exhibits a saturation of parametric instability and a restriction of the average velocity of motion in the laboratory reference system. In Section 6 the structure of the parameter space for the nonholonomic model and the system with viscous friction is compared and it is shown that the arrangements of regions of regular and chaotic dynamics are similar in both cases, as are the bifurcation scenarios leading to the onset of chaos.

## 1. BASIC EQUATIONS

The system under study is shown in Fig. 1 and is a platform of mass $m_0$ capable of moving on the plane. A particle of mass $m_p$ moves in a prescribed manner on the platform relative to it. We assume that the friction force is applied at the point of the platform, $R$, situated on the symmetry axis of the platform at distance $a$ from the center of mass of the platform $C$, and that the components of the friction force along and across the symmetry axis are proportional to the corresponding velocity components of point $R$ with greatly differing coefficients. To describe the motions, we will use two coordinate systems: a laboratory frame $Oxy$ and the frame $R\xi\eta$ attached to the platform.

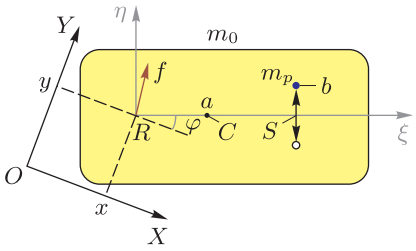


**Fig. 1.** The system under consideration. Friction is applied at point $R$ and is characterized by a large coefficient in the direction of the axis $\eta$ and a small (or zero) coefficient along the axis $\xi$, $C$ is the center of mass of the platform, the red arrow denotes the location of oscillations of the moving particle.

Let $u_1$ and $u_2$ be the projections of the velocity (measured in the laboratory frame) of point $R$ on the axis of the moving reference system, and let $\omega$ be the angular velocity of the platform. The kinetic energy of the platform together with the moving material point, which has coordinates $\xi_p(t)$, $\eta_p(t)$ in the moving reference frame, is

$$T = \frac{1}{2}m_0u_1^2 + \frac{1}{2}m_0(u_2 + a\omega)^2 + \frac{1}{2}J_0\omega^2 + \frac{1}{2}m_p(u_1 + \dot{\xi}_p - \eta_p\omega)^2 + \frac{1}{2}m_p(u_2 + \dot{\eta}_p + \xi_p\omega)^2, \quad (1.1)$$

where $J_0$ is the moment of inertia of the platform relative to the center of mass. We assume that the friction is characterized by the Rayleigh function

$$R = \frac{1}{2}c_1u_1^2 + \frac{1}{2}c_2u_2^2 + \frac{1}{2}c_3\omega^2, \quad (1.2)$$

where the coefficients $c_{1,2}$ are responsible for friction along the axes $\xi$ and $\eta$, and $c_3$ is responsible for friction with respect to the rotational motion.

The Lagrange equations can be written in a standard way as

$$\begin{aligned}
\frac{d}{dt}\left(\frac{\partial T}{\partial u_1}\right) &= \omega\frac{\partial T}{\partial u_2} - \frac{\partial R}{\partial u_1},\\
\frac{d}{dt}\left(\frac{\partial T}{\partial u_2}\right) &= -\omega\frac{\partial T}{\partial u_1} + \lambda - \frac{\partial R}{\partial u_2},\\
\frac{d}{dt}\left(\frac{\partial T}{\partial \omega}\right) &= u_2\frac{\partial T}{\partial u_1} - u_1\frac{\partial T}{\partial u_2} - \frac{\partial R}{\partial \omega}.
\end{aligned} \quad (1.3)$$

Introducing generalized momenta $P = \partial T/\partial u_1$, $Q = \partial T/\partial u_2$, $M = \partial T/\partial \omega$ and assuming $m = m_0 + m_p$, $\mu = m_p/m$, $I_0 = J_0/m$, $\xi_p = s$, $\eta_p = b\sin\Omega t$, we rewrite them as

$$\begin{aligned} \dot P &= \omega Q - \frac{c_1 u_1}{m}, \\ \dot Q &= -\omega P - \frac{c_2 u_2}{m}, \\ \dot M &= u_2 P - u_1 Q - \frac{c_3 \omega}{m}, \end{aligned} \tag{1.4}$$

where the quantities $u_1$, $u_2$, $\omega$ appearing on the right-hand sides are expressed in terms of $P$, $Q$, $M$ algebraically, via a system of linear equations.

Using dimensionless time $\tau = \Omega t$ and normalized variables $p = P/m\Omega$, $z = Q/m\Omega$, $q = M/m\Omega$, $u = u_1/\Omega$, $v = u_2/\Omega$, $w = \omega/\Omega$, we obtain

$$\begin{aligned} \dot p &= wz - \nu_1 u, \\ \dot z &= -wp - \nu_2 v, \\ \dot q &= vp - uz - \nu_3 w, \end{aligned} \tag{1.5}$$

$$\begin{pmatrix} 1 & 0 & -\mu b\sin\tau \\ 0 & 1 & D \\ -\mu b\sin\tau & D & J + \mu b^2\sin^2\tau \end{pmatrix} \begin{pmatrix} u \\ v \\ w \end{pmatrix} = \begin{pmatrix} p \\ z - \mu b\cos\tau \\ q - \mu s b\cos\tau \end{pmatrix}, \tag{1.6}$$

where $D = a - \mu a + \mu s$, $J = I_0 + a^2 + \mu(s^2 - a^2)$, $\nu_1 = c_1 m^{-1}\Omega^{-1}$, $\nu_3 = c_3 m^{-1}\Omega^{-1}$ and the dot denotes now the derivative with respect to dimensionless time $\tau$. We note that the equations are invariant under the change of variables

$$\tau \to \tau + \pi, \quad p \to p, \quad z \to -z, \quad q \to -q, \quad u \to u, \quad v \to -v, \quad w \to -w. \tag{1.7}$$

Suppose that at time $\tau = 2\pi n$ we are given the values of the variables $p_n$, $z_n$, $q_n$. Solving numerically with these initial conditions the equations in the time interval $\Delta\tau = 2\pi$, we can obtain new values

$$(p_{n+1}, z_{n+1}, q_{n+1}) = f(p_n, z_n, q_n). \tag{1.8}$$

Thus, we have defined a three-dimensional stroboscopic Poincaré map, which is convenient for description and representation of the results of analysis of the dynamical behavior.

Equations (1.5), (1.6) and the map (1.8), which govern the evolution of three variables $p$, $z$, $q$, respectively, in continuous and discrete time, define the reduced system, which can be considered independently of the other variables relating to configuration space. The coordinates of the point of application of friction, $R$, in the laboratory reference system, $X$ and $Y$, and the angle of rotation of the platform, $\varphi$, obey the equations supplementing the system (1.3):

$$\dot x = u\cos\varphi, \quad \dot y = u\sin\varphi, \quad \dot\varphi = \omega, \tag{1.9}$$

which completes the mathematical formulation of the problem.

For the Chaplygin sleigh, where the nonholonomic constraint, which ensures that the velocity component in the direction of the axis $\eta$ is zero, is assumed to be imposed instead of viscous friction at point $R$, one should write, instead of Eqs. (1.5) and (1.6), using the same notation, the following equations:

$$\begin{aligned} \dot p &= (Dw + \mu b\cos\tau)w - \nu_1 u, \\ \dot q &= -(Dw + \mu b\cos\tau)u - \nu_3 w, \end{aligned} \tag{1.10}$$

$$\begin{pmatrix} 1 & -\mu b\sin\tau \\ -\mu b\sin\tau & 1 \end{pmatrix} \begin{pmatrix} u \\ w \end{pmatrix} = \begin{pmatrix} p \\ q - \mu s b\cos\tau \end{pmatrix}. \tag{1.11}$$

Formally, these equations are obtained from (1.5) and (1.6) by simply excluding the equation for the transverse velocity, setting this velocity equal to zero, $v = 0$, and using the relation, following

from (1.6), for the transverse component of the generalized momentum: $z = Dw + \mu b \cos\tau$. An accurate transition is made by considering the system of interest within the framework of the concepts of fast-slow motions, taking into account the large coefficient of transverse friction, which was done previously by Fufaev [29, 30] for the case of free motion of the Chaplygin sleigh. Such a passage to the limit involves using the methods developed for differential equations with a small parameter at a higher derivative [49–51], in particular, in the context of the concept of a boundary layer in hydrodynamics problems. The main result in this vein is the well-known Tikhonov theorem, which establishes conditions under which the system can be adequately described by equations obtained by eliminating the term with a small parameter at the derivative, due to the fact that for the complete system in the space of states the solutions approach fast the surface of slow motions, which corresponds to the space of states of the asymptotic problem. In [27, 28, 52–54], attention is given to the development of this approach for problems of nonholonomic mechanics. According to the recent paper by Eldering [54], the fact that the dynamics within the framework of a complete description corresponds to the dynamics within the framework of asymptotic equations obtained on the basis of the Tikhonov theorem may be asserted with confidence only on finite times of observation. Below we will make special note of this when discussing comparative results of numerical simulation of the dynamics of our system on the basis of the nonholonomic model and the model with friction. A derivation of Eqs. (1.10) and (1.11) within the framework of the nonholonomic model is presented in [16–18].

## 2. SELF-ACCELERATION UNDER SMALL OSCILLATIONS OF THE INTERNAL MASS

We start by discussing the effect of acceleration of the motion of the platform in the case where the amplitude of periodic oscillations of the particle is small and its mass is small relative to the mass of the platform. For the nonholonomic model of the Chaplygin sleigh (1.10), (1.11) this effect was considered in [16]. It was shown that in certain parameter regions the motion occurs in the direction of the longitudinal axis of the sleigh with velocity increasing with time as $\tau^{1/3}$. The corresponding regions on the parameter plane where acceleration takes place are shown in grey in Fig. 2. The distance from the point of application of the constraint to the location of the particle's oscillation is plotted along the abscissa axis, and the relative mass of the particle is plotted along the ordinate axis, with the other parameters fixed.

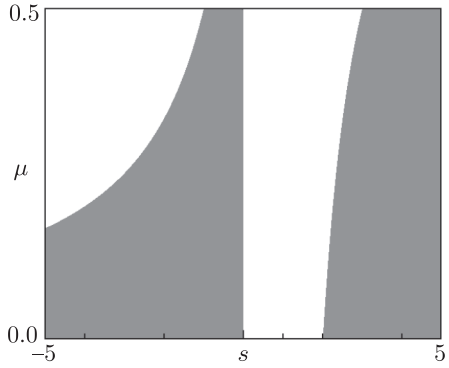


**Fig. 2.** Regions of unbounded acceleration of the Chaplygin sleigh due to small periodic oscillations of the internal mass (grey) and regions of bounded variation of generalized velocities (white) on the plane of parameters $s$, $\mu$ for $J_0 = 1$, $a = 1$, $b = 0.2$ according to [16].

Numerical calculations show that the effect consisting in the acceleration of the directed motion of the platform persists when the nonholonomic constraint is replaced by transverse viscous friction. Figure 3 presents diagrams illustrating this effect and comparing the nonholonomic model in the absence of friction (1.10), (1.11) and the model with transverse viscous friction (1.5), (1.6) for different values of the coefficient $\nu_2$ (lines). For both models, the figure shows time dependences of the combination $\frac{1}{3}D^2p^3 + J^2p$, which, in accordance with the asymptotic method developed in [16], increases linearly in the case of a nonholonomic constraint and in the absence of friction. It can be seen that, if the coefficient of transverse friction is sufficiently large, then the dependence in the

initial interval in the model with friction is close to the dependence predicted by the nonholonomic model. However, with the passage of time, the increase in the velocity slows down as compared to the nonholonomic model and has the tendency to saturation. The same effect was pointed out in [18] for the case where small friction in the longitudinal direction and friction for the rotational motion of the platform are incorporated into the nonholonomic model. The influence of the corresponding effects on self-acceleration in the model with transverse viscous friction is illustrated in Fig. 4: the effect of saturation becomes more pronounced.

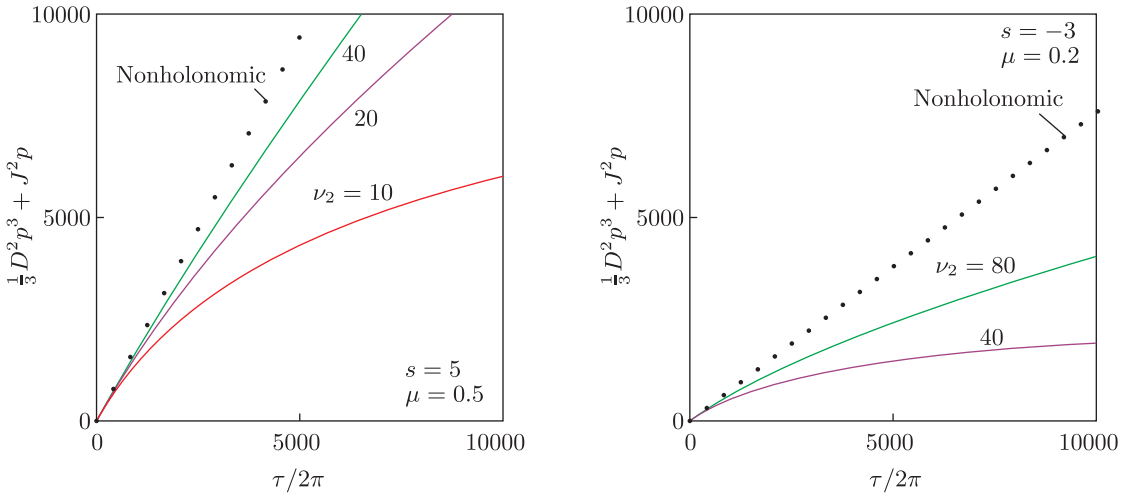


**Fig. 3.** Diagrams illustrating the acceleration of the motion of the platform for small oscillations and a small mass of the particle: comparison of the nonholonomic model in the absence of friction (dots) and the model with transverse friction for different values of the friction coefficient $\nu_2$ (lines). The diagrams show the dependence of the combination $\frac{1}{3}D^2p^3 + J^2p$ on dimensionless time for two cases, $s = 5$, $\mu = 0.5$ and $s = -3$, $\mu = 0.2$, when unbounded acceleration takes place in the nonholonomic model. The other parameters are: $I_0 = 1$, $a = 1$, $b = 0.2$.

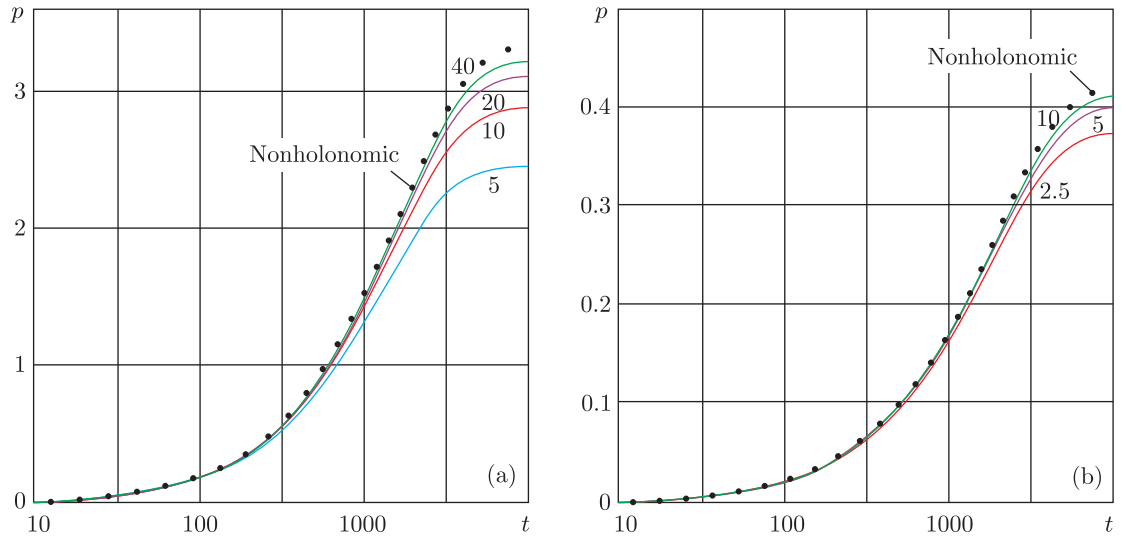


**Fig. 4.** Dependence of the dimensionless longitudinal momentum $p$ on dimensionless time in parameter regions corresponding to the acceleration of the motion of the platform for the nonholonomic model (dots) and for the system with small longitudinal and large transverse viscous friction — solid lines, close to which the values of the transverse friction coefficient are presented: (a) $s = -1$, $\mu = 0.4$, (b) $s = 5$, $\mu = 0.3$. The other parameters are: $J_0 = 1$, $a = 1$, $b = 0.3$, $\nu_1 = 0.001$, $\nu_3 = 0.2$.

The results obtained in this section provide a clear illustration of the applicability of the Tikhonov theorem [49, 50, 54]. Namely, considering the specific system described within the

framework of the nonholonomic model and the model with friction, one can see that the correspondence taking place on finite times of observation can be violated in the sense that asymptotically steady motions can be different.

## 3. FRACTAL AND FAT CHAOTIC ATTRACTORS AND HOW THEY ARE TRANSFORMED IN THE MODEL WITH TRANSVERSE FRICTION

With increasing amplitude of oscillations of the moving mass, which is characterized by parameter $b$, the model equations exhibit more complex dynamics. In particular, in certain parameter regions one observes chaotic dynamics corresponding to strange attractors [16–18]. Examples of such attractors are given in Fig. 5.

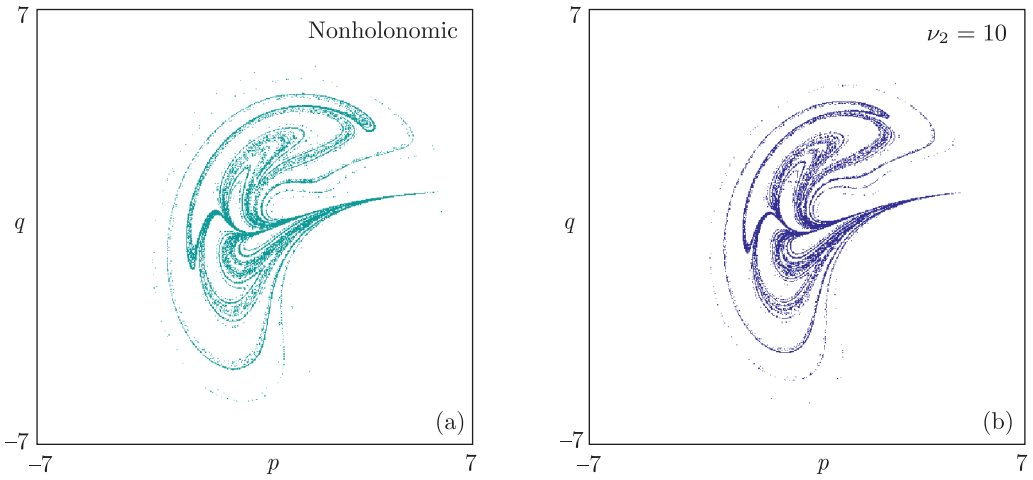


**Fig. 5.** Portraits of an attractor in the stroboscopic section for the model with a nonholonomic constraint (a) and for a system with friction for $\nu_2 = 10$ (b). The other parameters are: $J_0 = 1$, $a = 1$, $s = 0.9$, $\mu = 0.5$, $b = 3$.

It should be noted that for the nonholonomic model without friction the existence of attractors is not quite trivial, since the system possesses symmetry with respect to time reversal and, in the absence of oscillations of the internal mass, conserves the mechanical energy. However, even in a simple case such as the free motion of the Chaplygin sleigh, the reduced equations exhibit attractors in the form of fixed points, which are neutral with respect to the perturbation of energy [11, 12]. The possibility of existence of chaotic attractors in systems of nonholonomic mechanics was first pointed out by Borisov and Mamaev (for rattleback-type systems) [44], see also [45, 46]. The presence of symmetry with respect to time reversal means that each attractor corresponds to a symmetric partner which is a repeller, i. e., an attractor of the system with reversed time.

The diagram in Fig. 5 on the left demonstrates a strange attractor of the nonholonomic model of the Chaplygin sleigh with periodic oscillations of a massive particle, which was found in [16]. The attractor is presented in the stroboscopic section on the plane $(p, q)$. The Lyapunov exponents calculated for the Poincaré map[2)] are

$$\Lambda_1 = 0.49, \quad \Lambda_2 = -2.45.$$

Thus, we obtain the Kaplan – Yorke dimension [33, 34, 47] $D_{KY} \approx 1.2$.

The diagram in Fig. 5 (right) shows a strange attractor of the model with transverse viscous friction. In this case, the Poincaré map is three-dimensional. The image is presented as a projection from the three-dimensional space of states $(p, z, q)$ onto the plane $(p, q)$, which allows a clear visual comparison with the nonholonomic model. As can be seen, both portraits of the attractors

[2)] The Lyapunov exponents were calculated by the standard method [33, 34, 48] for a map for a period on the basis of the numerical solution of Eqs. (1.5), (1.6) for models with friction and Eqs. (1.10), (1.11) for the nonholonomic model together with the corresponding linearized equations in variations and orthogonalization of the Gram – Schmidt perturbation vectors in each step of the Poincaré map.

demonstrate a remarkable similarity. The Lyapunov exponents found numerically for the attractor of the system with friction are

$$\Lambda_1 = 0.54, \quad \Lambda_2 = -2.05, \quad \Lambda_3 = -35.26.$$

As can be seen, two largest Lyapunov exponents are in good quantitative agreement with the exponents for the nonholonomic model. The Kaplan – Yorke dimension of the attractor is $D_{KY} \approx 1.26$, which is also close to the value for the nonholonomic model.

The charts of the parameter plane shown in Fig. 6 give a general idea of possible modes of the model systems of interest. The color denotes the value of the largest Lyapunov exponent.

The left diagram (a) reproduces a chart for the nonholonomic model without friction, as obtained in [18]. For comparison, the middle panel shows a chart (b) for the model where, instead of the nonholonomic constraint, transverse friction takes place with the coefficient $\nu_2 = 10$. Both charts have been plotted by scanning pixels in the region on the parameter plane in such a way that for each pixel the calculation of the trajectory and the calculation of the Lyapunov exponent start under the same initial conditions.

In yellow and light-red regions, the dynamics for the nonholonomic model is observed which is similar to the situation of Hamiltonian systems [35–37] where on the phase plane there coexist the region of a "chaotic sea" and regions of regular motions represented by invariant curves. (Under initial conditions given in plotting the chart, motions relating to the "chaotic sea" are observed.) In [18] it is noted that, in contrast to the usual conservative systems, the positive and negative Lyapunov exponents in the nonholonomic model are different, and therefore the chaotic sea is qualified as a specific type of attractor, the so-called "fat attractor". For the system with friction the diagram in panel (b) uses coloring in accordance with the Lyapunov exponent for a transitional trajectory calculated on the segment of the trajectory with the same initial conditions. This allows a comparison of the motion pattern on a finite time of observation, which is in remarkable agreement for the nonholonomic model and the model with friction. However, it should be kept in mind that for the model with friction this gives no correct idea of the pattern of asymptotically steady motions. In the above-mentioned regions, after a long transitional process the motions of the system become regular and periodic, and correspond in the stroboscopic map to successive visiting of a finite set of points.

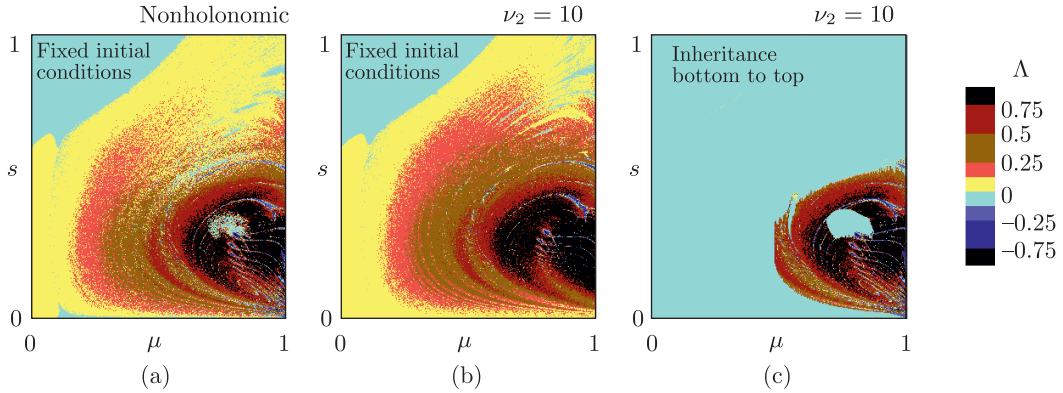


**Fig. 6.** Charts on the parameter plane of the nonholonomic model (a) and of the model with transverse viscous friction (b, c) for $\nu_2 = 10$, where the colors denote values of the largest Lyapunov exponent of the stroboscopic map (the legend on the right). Charts (a) and (b) have been plotted under the initial conditions which are the same for each point of the parameter plane, and chart (c) has been constructed when scanning in the direction from bottom to top with inheritance of the initial state at each new point according to the final state at the preceding point. The other parameters are: $a = 0.5$, $J_0 = 0.05$, $b = 1$, $\nu_1 = \nu_3 = 0$.

On the other hand, in the lower right part of the chart shown in Fig. 6a, the system exhibits chaos, which is associated with a strange attractor analogous to the attractors of dissipative systems (a "thin", or fractal attractor). This is the same type of attractors as in Fig. 5. Such attractors persist when passing from the nonholonomic system to the model with friction.

The chart in Fig. 6c provides insight into the nature of the steady-state modes depending on the parameters in the model with friction. This chart has been plotted by scanning the parameter

plane, pixel after pixel, in the direction from bottom to top with inheritance: the initial conditions in calculations for a new pixel are given as a set of variables obtained at the end of calculations for the preceding pixel. Instead of the yellow and light-red regions, an extensive light-blue region is observed, which corresponds to periodic modes with negative Lyapunov exponents.

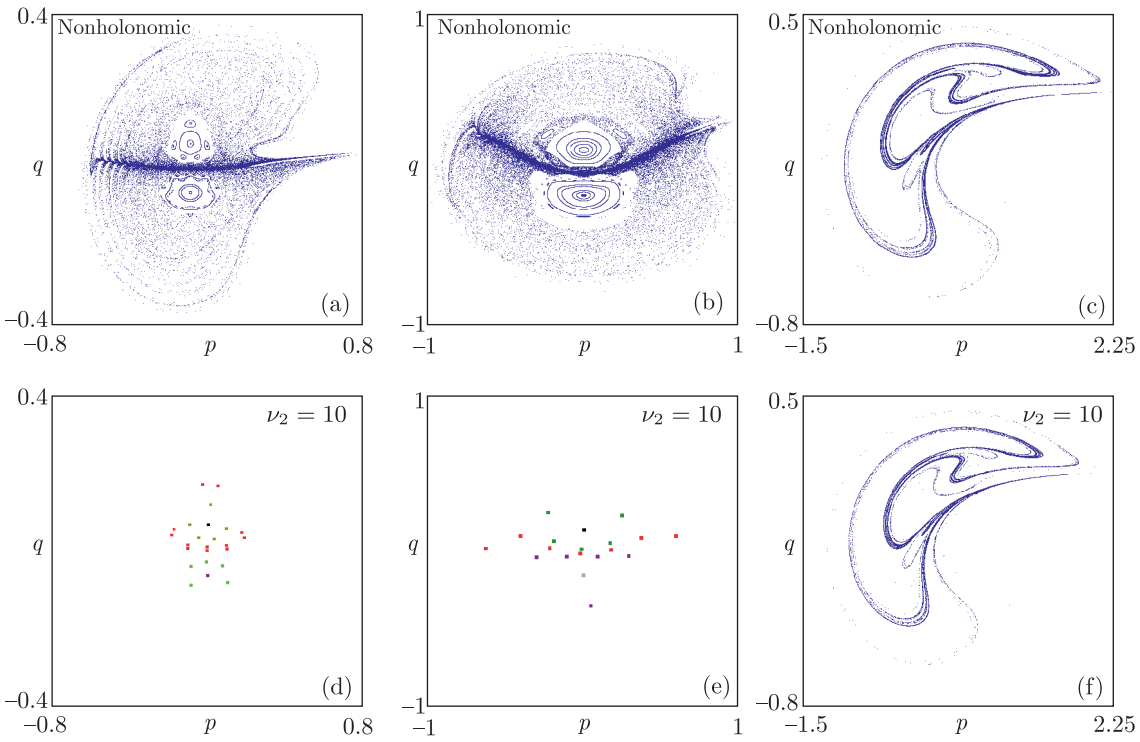


**Fig. 7.** Phase portraits of a reduced system in the stroboscopic section for $s = 0.25$, $\mu = 0.25$ (a, d), $s = 0.75$, $\mu = 0.75$ (b, e) and $s = 0.25$, $\mu = 0.75$ (c, f). The upper row corresponds to the nonholonomic model (1.10), (1.11), and the lower row corresponds to the model with transverse viscous friction (1.5), (1.6) with $\nu_2 = 10$. The coexisting attracting periodic motions in the diagrams (d, e) are indicated by dots of different colors. The first two diagrams relate to situations of coexistence of a "fat attractor" and invariant curves on the phase plane $(p, q)$, and the third demonstrates a "thin" strange attractor. The lower row corresponds to the system with transverse friction with the coefficient $\nu_2 = 10$.

Figure 7 shows phase portraits in the stroboscopic section at representative points on the parameter plane of Fig. 6. The upper row corresponds to the nonholonomic model, where the first two diagrams relate to coexistence of a "fat attractor" and invariant curves on the phase plane $(p, q)$, and the third demonstrates a "thin" strange attractor. The lower row corresponds to the system with transverse friction with the friction coefficient $\nu_2 = 10$. These are projections from the three-dimensional phase space $(p, z, q)$ onto the plane $(p, q)$. If one compares these diagrams with the corresponding pictures from the upper row, one can see that, instead of the "fat attractors" and regular motions occurring in the nonholonomic model, coexisting attracting cycles are formed in the model with friction. (The type of the attracting cycle arising for the system is determined by the initial conditions.) On the other hand, the fractal strange attractor looks remarkably similar for the system with friction and for the nonholonomic model. This manifests itself not only in the visual similarity, but also quantitatively; indeed, the Lyapunov exponents of the nonholonomic model

$$\Lambda_1 = 0.846, \quad \Lambda_2 = -5.10$$

are close in value to the first two Lyapunov exponents of the model with friction

$$\Lambda_1 = 0.845, \quad \Lambda_2 = -4.89, \quad \Lambda_3 = -37.00.$$

The values of the Kaplan – Yorke dimension are in both cases also close to each other (approximately 1.17).

## 4. TWO-DIMENSIONAL RANDOM WALK IN THE LABORATORY REFERENCE SYSTEM

Dynamical modes associated with the strange attractors of reduced equations correspond to motion of the platform in the laboratory reference system in the form of two-dimensional random walks, without a preferred direction and with the loss of memory of the initial orientation for large time scales [38–40]. Also, the distribution of distances from the beginning to the end of the segment of the trajectory traveled within a fixed number of oscillations of the internal mass $N$ (the number of iterations of the Poincaré map) is characterized by the Rayleigh distribution function, and the distribution of the azimuth angles of rotation tends to uniform distribution. For the nonholonomic model this circumstance is pointed out in [16, 18].

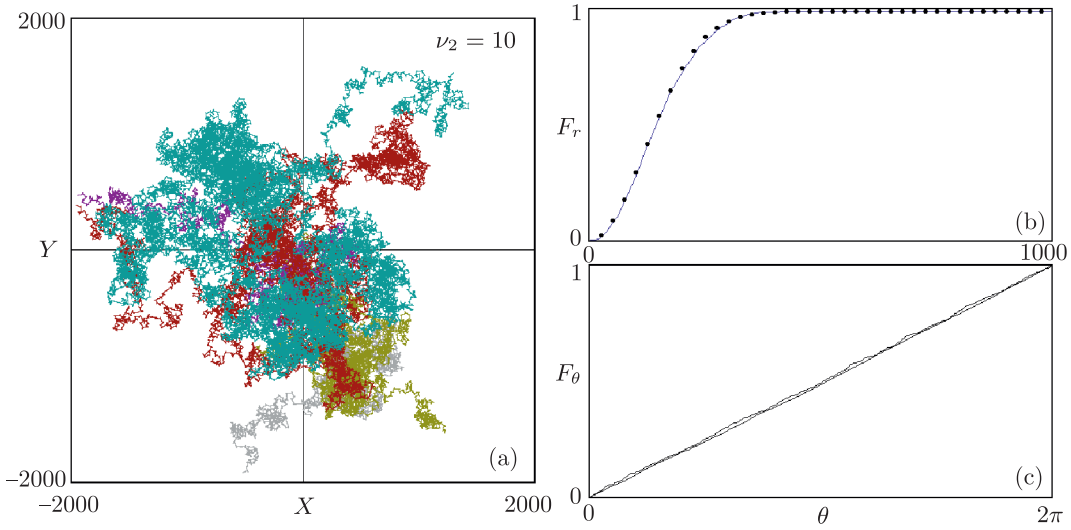


**Fig. 8.** A family of fragments of the trajectory in the laboratory reference system for the model with transverse friction with the coefficient $\nu_2 = 10$, which are visualized as described in the text (a) and cumulative distribution functions for the traveled distances and azimuth angles (b, c) obtained for $1.7 \cdot 10^3$ iterations of the Poincaré map. In diagram (b), the data are compared with the Rayleigh distribution (dots), and diagram (c) is indicative of a uniform distribution of the azimuth angles. The other parameters are: $a = 1$, $\Omega = 1$, $J_0 = 1$, $\mu = 0.5$, $b = 3$, $s = 0.9$, $\nu_1 = \nu_3 = 0$.

Figures 8 and 9 illustrate a random walk and its statistical characteristics for the model with friction; for comparison, Fig. 10 shows analogous results pertaining to the nonholonomic model.

Diagrams (a) show what the trajectory of the center of mass of the platform on the plane $(X, Y)$ looks like when parameters corresponding to the strange attractor of the reduced equations are specified. The graphs have been plotted by integrating equations for the coordinates (1.9) together with the reduced equations, respectively, (1.5), (1.6), and (1.9), (1.10). The start is performed from the origin of coordinates $x = 0$, $y = 0$ with zero initial conditions for generalized velocities and with a zero initial angle of rotation. The motion is tracked until the instant when the distance from the origin of coordinates exceeds the specified value $r_{\max} = 2000$. Further, the calculations are continued with current values of the generalized velocities and the rotation angle, but with a start again from the origin of coordinates. Thus, the diagrams show several successive fragments of the same trajectory corresponding to the orbit of the reduced equations which approaches to a chaotic attractor.

Diagrams (b) and (c) show cumulative distributions for the distances

$$r = \sqrt{(x_{(k+1)N} - x_{kN})^2 + (y_{(k+1)N} - y_{kN})^2}$$

and the angles $\theta = \arg[(x_{(k+1)N} - x_{kN}) + i(y_{(k+1)N} - y_{kN})]$. The solid lines correspond to numerical results for the specified number of periods, $N = 150$. The role of the sample space is played by the set whose elements are the fragments of the above-mentioned reference trajectory, labeled by the index $k = 1 \ldots 10^4$.

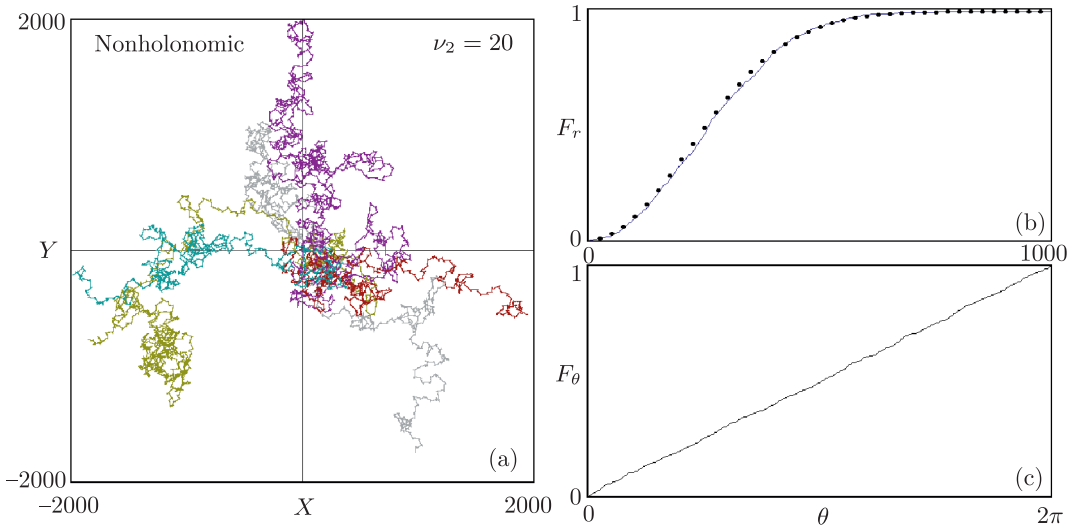


**Fig. 9.** A family of fragments of the trajectory in the laboratory reference system for the model with transverse friction with the coefficient $\nu_2 = 20$, which are visualized as described in the text (a) and cumulative distribution functions for the traveled distances and azimuth angles (b, c), obtained for $10^3$ iterations of the Poincaré map. In diagram (b), the data are compared with the Rayleigh distribution (dots), and diagram (c) is indicative of a uniform distribution of the azimuth angles. The other parameters are: $a = 1$, $\Omega = 1$, $J_0 = 1$, $\mu = 0.5$, $b = 3$, $s = 0.9$, $\nu_1 = \nu_3 = 0$.

The dots in panel (b) correspond to the Rayleigh distribution $F(r) = 1 - e^{-r^2/2\sigma^2}$, where $2\sigma^2$ is the sum of variances of the random quantities $x_{(k+1)N} - x_{kN}$ and $y_{(k+1)N} - y_{kN}$, obtained as statistical estimates from the available samples. The value of the variance at $\nu_2 = 10$ is $\sigma^2 \approx 1.44 \cdot 10^4$, for $\nu_2 = 20$ we have $\sigma^2 \approx 4.65 \cdot 10^4$, and for the nonholonomic model the variance is $\sigma^2 \approx 1.05 \cdot 10^5$. Using the well-known relation from the theory of two-dimensional random walks, one can estimate the diffusion coefficient as the ratio of this value to the corresponding double time interval: $D = \sigma^2/4\pi N$, which gives for the three above-mentioned cases, respectively, 7.6, 24.7, and 55.7. Thus, the velocity of diffusion increases appreciably as the coefficient of longitudinal friction increases and as one passes to the situation where the nonholonomic model is applicable, although the attractors of the reduced equations look very similar.

The distributions for azimuth angles in diagrams (c) are evidently close to a uniform distribution.

## 5. THE MECHANISM OF ACCELERATION CAUSED BY PARAMETRIC RESONANCE

The next effect we discuss here is the mechanism of acceleration of the system's motion with increasing mechanical energy of the platform, which is related to parametric resonance and excitation of oscillations.

As pointed out in [18], in a particular case of the nonholonomic model, when the oscillating particle moves perpendicularly to the principal axis $\xi$ in a straight line passing through the center of mass of the entire system (platform plus particle), the problem reduces, taking longitudinal friction into account, to a system of linear equations with variable coefficients. In this situation, the effect of unbounded parametric excitation of oscillations like that in the Mathieu equation [41–43] is possible in certain parameter regions. We note that the presence of friction in the longitudinal direction is a necessary condition for the onset of this effect.

As numerical calculations show, the modification of the phenomenon of parametric acceleration in the model where the nonholonomic constraint is replaced by strong transverse viscous friction is that the observed growth of the kinetic energy is stabilized at a certain level. The larger the coefficient of transverse friction, the higher this level. Figure 11 shows diagrams illustrating the behavior of the phase trajectory of the system in the situation of parametric acceleration for the nonholonomic model (panel (a)) and the model with strong transverse viscous friction with the coefficient $\nu_2 = 80$ (panel (b)). As can be observed, in the latter case, the system exhibits, instead of unbounded acceleration, a regular attractor, which is represented in the Poincaré section of the closed invariant curve in the form of a figure-of-eight. The motion on this attractor corresponds

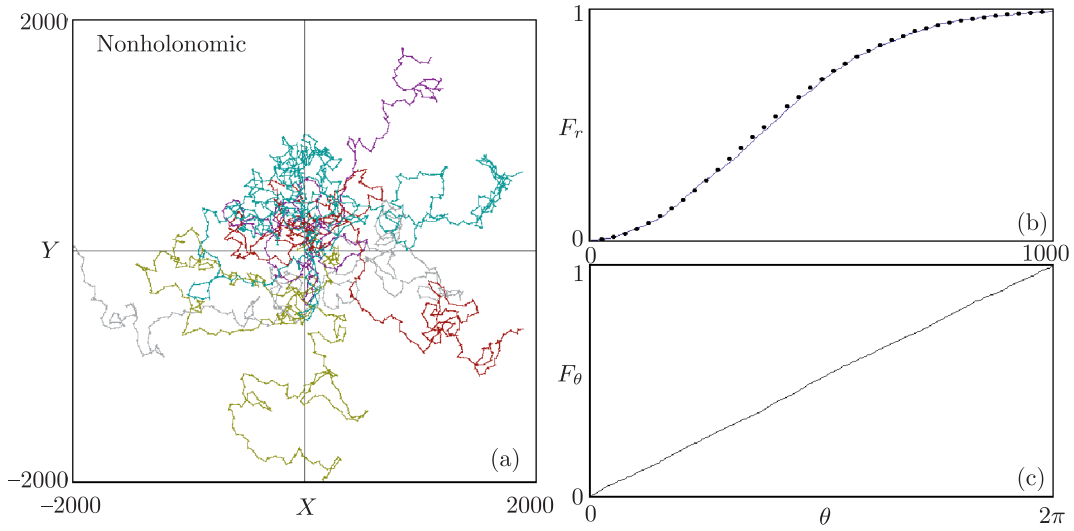


**Fig. 10.** A family of fragments of the trajectory in the laboratory reference system for the nonholonomic model, which are visualized as described in the text (a), and cumulative distribution functions for the traveled distances and azimuth angles (b, c), obtained for $1.1 \cdot 10^3$ iterations of the Poincaré map. In diagram (b), the data are compared with the Rayleigh distribution (dots), and diagram (c) is indicative of a uniform distribution of the azimuth angles. The other parameters are: $a = 1$, $\Omega = 1$, $J_0 = 1$, $\mu = 0.5$, $b = 3$, $s = 0.9$, $\nu_1 = \nu_3 = 0$.

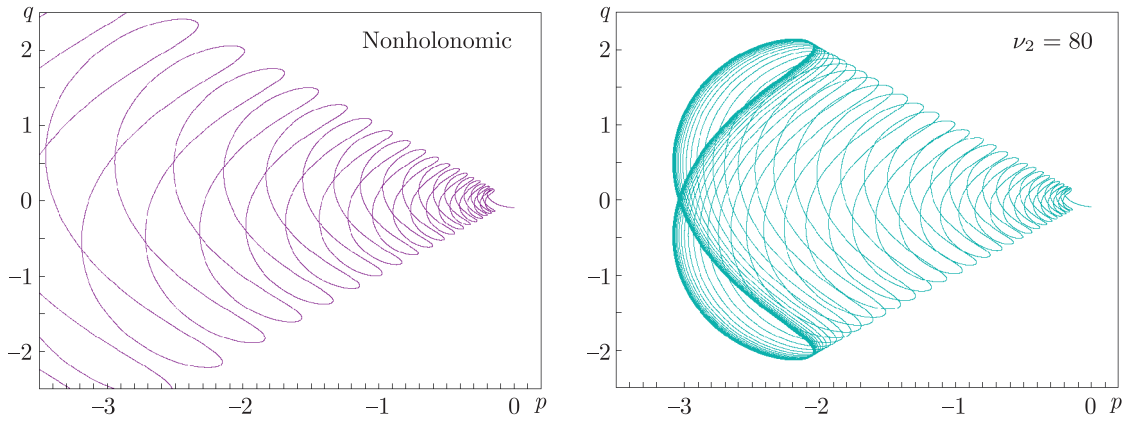


**Fig. 11.** Parametric acceleration: comparison of the nonholonomic case and the model with transverse friction for $\nu_2 = 80$. The other parameters are: $\Omega = 1$, $b = 1$, $J_0 = 0.15$, $a = 0$, $s = 0$, $\nu_1 = 0.35$, $\nu_3 = 0.1$, $\mu = 0.85$. The initial conditions are: $p = 0$, $z = 0$, $q = -0.1$.

in the laboratory coordinate system to directed motion of the platform, which is accompanied by strong oscillations across the direction of averaged motion (Fig. 12). The averaged motion occurs in the steady-state mode with constant average velocity the direction of which depends on the spatial orientation of the platform in the case of a start in the laboratory reference system.

The restriction of the effect of parametric excitation of oscillations, and hence the velocity with which the platform gains the kinetic energy, can be attributed to the fact that the transverse component of the reaction force of the medium, the role of which is played by the transverse component of the viscous friction force, turns out to be bounded. This is illustrated in Fig. 13, where the time dependence of the reaction force is compared in the nonholonomic model and in the model with transverse viscous friction for motions along the phase trajectories shown in Fig. 11, respectively, in panels (a) and (b).

## 6. PARAMETER SPACE TOPOGRAPHY AND BIFURCATION SCENARIO

We now discuss in more detail the dynamical modes which can, depending on the parameters, take place in a system with large transverse and small longitudinal viscous friction, in comparison with the nonholonomic model.

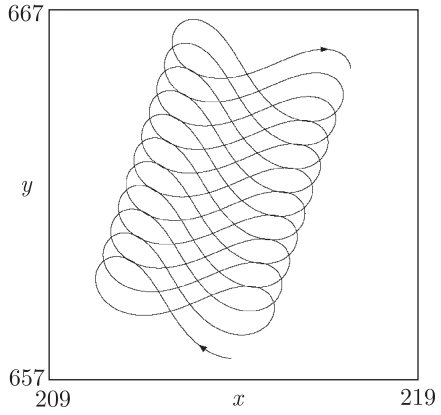


**Fig. 12.** Trajectory of the center of mass in the laboratory reference system in the steady-state mode of motion resulting from parametric acceleration in the model with friction. The parameters are: $\Omega = 1$, $b = 1$, $J_0 = 0.15$, $a = 0$, $s = 0$, $\nu_1 = 0.35$, $\nu_2 = 80$, $\nu_3 = 0.1$, $\mu = 0.85$. The initial conditions are: $p = 0$, $z = 0$, $q = -0.1$, $x = 0$, $y = 0$, $\varphi = \pi/2$.

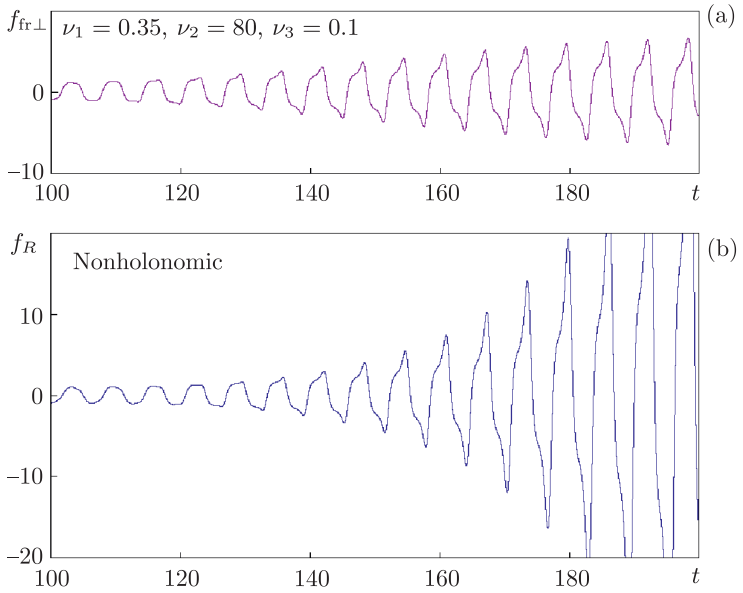


**Fig. 13.** Time dependence of the dimensionless transverse component of the viscous friction force in the system with the coefficient of transverse friction $\nu_2 = 80$ (a) and the reaction force in the system with the nonholonomic constraint (b) in the process of parametric acceleration. The center of mass of the platform coincides with the place of application of friction (the position of the knife edge), i. e., the parameter $a = 0$, and the oscillations of the point mass occur on the line passing through the center of mass, i. e., $s = 0$. The other parameters are: $I_0 = 0.15$, $\mu = 0.85$, $b = 1$, $\nu_1 = 0.35$, $\nu_3 = 0.1$.

Figure 14 shows charts of modes on the parameter plane of the relative mass of an oscillating particle $\mu$ and the coefficient of longitudinal friction $\nu_1 = 0.1$ for the system with transverse viscous friction $\nu_2 = 20$ and for the nonholonomic model. Different colors indicate periodic modes, and white denotes the region of chaos in accordance with the legend shown on the right. As can be seen, the general arrangement of the regions in both charts demonstrates an obvious similarity, although in the chart for the system with transverse friction the region of complex dynamics and chaos is significantly shifted downward. In fact, as the coefficient of transverse friction increases, this region shifts upward, and the picture becomes similar to that which corresponds to the nonholonomic model.

Figure 15 presents bifurcation diagrams for the values of the dynamical variable $q$ (dimensionless angular momentum), which correspond to the attractor of the Poincaré map, versus the parameter of the relative value of the oscillating mass $\mu$, and presents graphs showing the dependence of the largest Lyapunov exponent for the system with transverse friction and for the nonholonomic model in the same interval of the parameter. On the parameter plane of Fig. 14, this corresponds

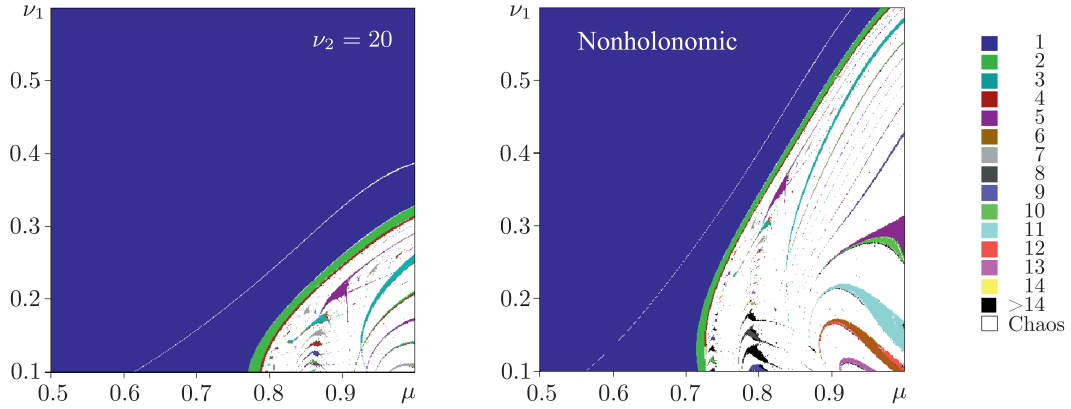


**Fig. 14.** Charts of modes for the model with transverse friction for $\nu_2 = 20$ and for the nonholonomic model. The other parameters are: $\Omega = 1$, $b = 1$, $J_0 = 0.15$, $a = 0$, $s = 0.1$, $\nu_3 = 0.1$.

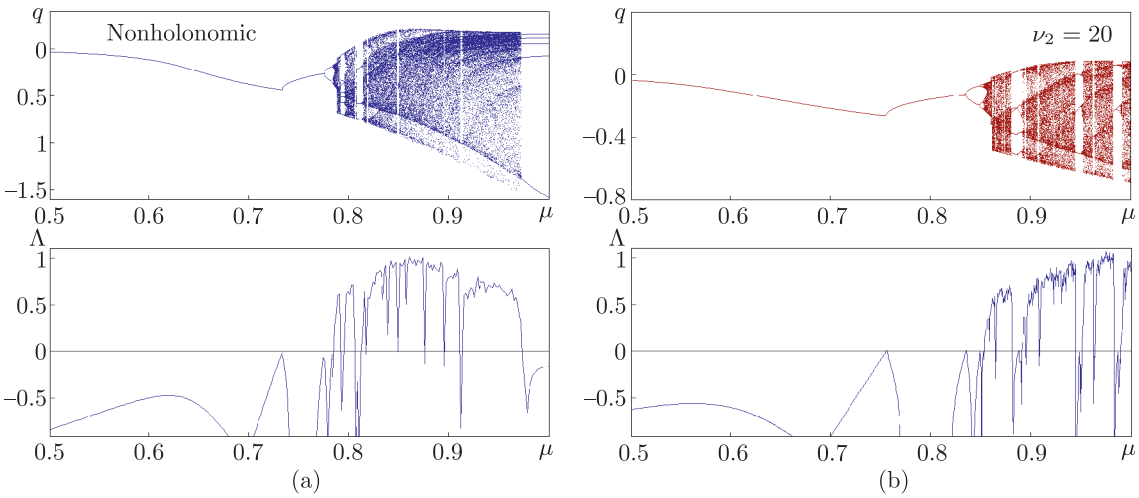


**Fig. 15.** Bifurcation trees and dependences of the largest Lyapunov exponent on the parameter of the ratio of masses: (a) the nonholonomic model for $\nu_1 = 0.3$, $\nu_3 = 0.1$, (b) the model with transverse friction for $\nu_1 = 0.2$, $\nu_2 = 20$, $\nu_3 = 0.1$. The other parameters are: $s = 0.1$, $a = 0$, $\Omega = 1$, $J_0 = 0.15$, $s = 0.1$.

to passage along the horizontal line $\nu_1 = \text{const}$. As can be seen, the diagrams for the model with transverse friction and for the nonholonomic model demonstrate an obvious similarity, but with values of the coefficient of longitudinal friction shifted relative to each other.

Figure 16 depicts attractors of the system with continuous time for the model with friction at representative points on the axis of parameter $\mu$, and shows, against this background, points (colored dark) corresponding to the stroboscopic Poincaré section, i. e., to time instants $\tau_n = 2\pi n$. Each panel has a caption indicating the Lyapunov exponents of the Poincaré map which have been found numerically for the corresponding attractor.

During motion along the axis of parameter $\mu$ from left to right we first observe an attractor in the form of a symmetric loop (figure-of-eight), which corresponds to the attracting fixed point of the Poincaré map (panel (a)). Then, at $\mu \approx 0.754$, the system undergoes a bifurcation of the symmetry loss of the solution relative to the change of variables (1.7), followed by a cascade of period-doubling bifurcations (panels (b) and (c)), and a transition to chaos. The resulting chaotic attractor is first asymmetric (d), so that in the phase space it coexists with a symmetric attractor obtained by the change of variables (1.7). As the parameter increases, the attractor and its partner merge to form a single symmetric attractor (e). Such symmetric attractors can be seen in panels (g) and (i); on the other hand, panel (h) demonstrates an asymmetric chaotic attractor. The region of chaos is interspersed with periodicity windows, which look like light-colored vertical strips in the bifurcation diagram and like dips into the negative region on the graph of the Lyapunov exponent. The attractor shown in panel (f) corresponds to one of the regularity windows. The sequence

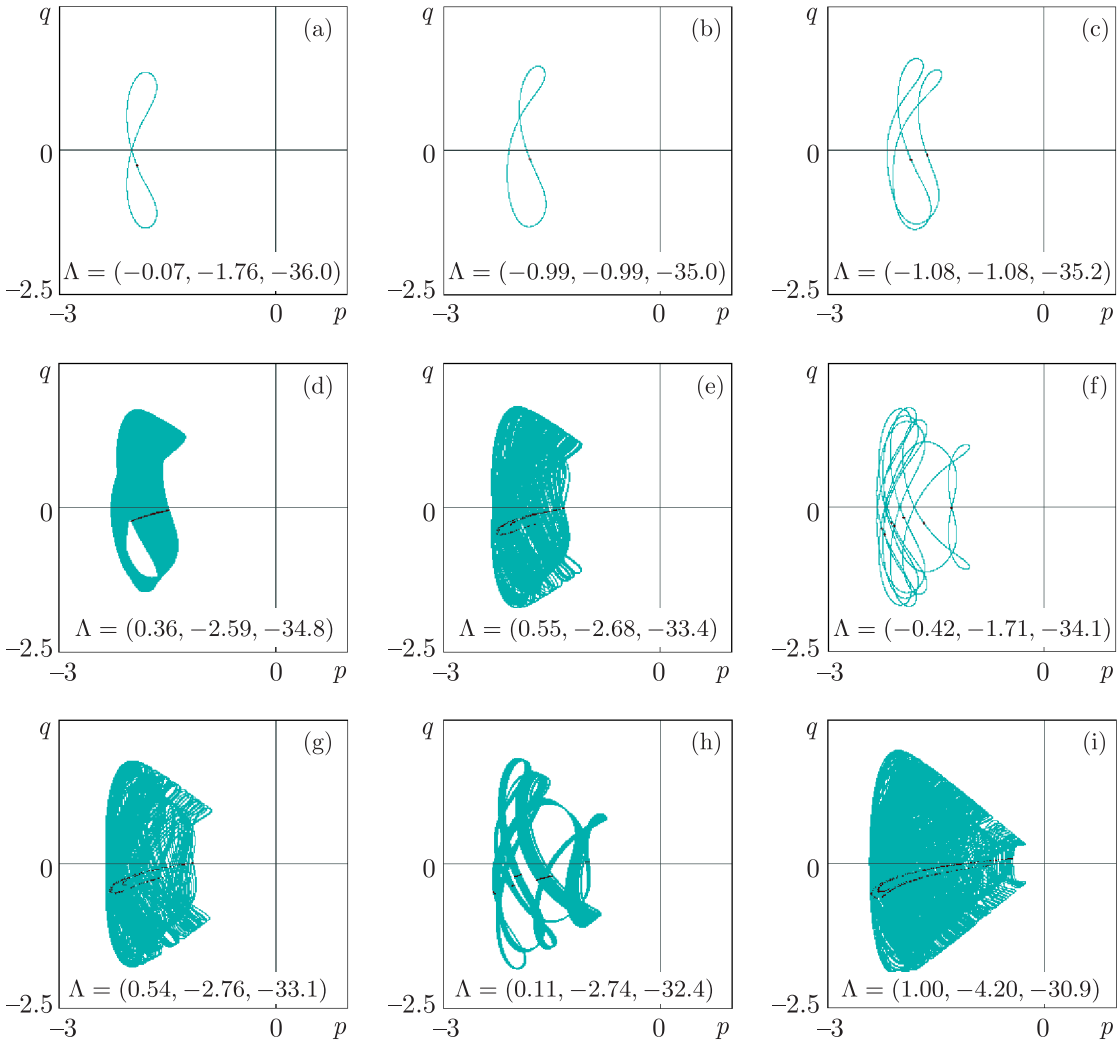


**Fig. 16.** Attractors of the reduced equations of the system with large transverse and small longitudinal viscous friction for the parameters $I_0 = 0.15$, $\nu_1 = 0.2$, $\nu_3 = 0.1$, $\varepsilon = 1$, $a = 0$, $s = 0.1$ and $\mu = 0.75$ (a), 0.8 (b), 0.84 (c), 0.856 (d), 0.86 (e), 0.8635 (f), 0.875 (g), 0.891 (h), 0.94 (i). Light-blue denotes the trajectories in continuous time, and red indicates points corresponding to the stroboscopic Poincaré section at times $t = 2\pi n$. The Lyapunov exponents of the stroboscopic map are shown near the portraits of attractors.

of bifurcations described above reproduces the sequence discussed in [18] for the nonholonomic model, although the best agreement takes places when the coefficient of longitudinal friction $\nu_1$ in the nonholonomic model is somewhat increased.

In the system with longitudinal friction, the difference between the nonholonomic model and the model with transverse friction is not so great as the difference that was observed in the situation without longitudinal friction and manifested itself in a transition from quasi-conservative dynamics (when there coexisted a "fat attractor" and regularity regions occupied by invariant curves) to multistability. In the system with longitudinal friction the dynamics of the nonholonomic model and that of the model with transverse viscous friction are in much better qualitative agreement with each other. This can be seen by comparing the charts of Lyapunov exponents presented in Fig. 17, which are remarkably similar to each other.

## CONCLUSION

In this paper, we have considered the problem of the motion of a rigid body (platform) on a plane, initiated by oscillations of a point mass relative to the body, in the presence of the viscous friction force applied at a fixed point of the platform and having in a specific direction relative to the platform a small value and a large value in the transverse direction. This problem is analogous

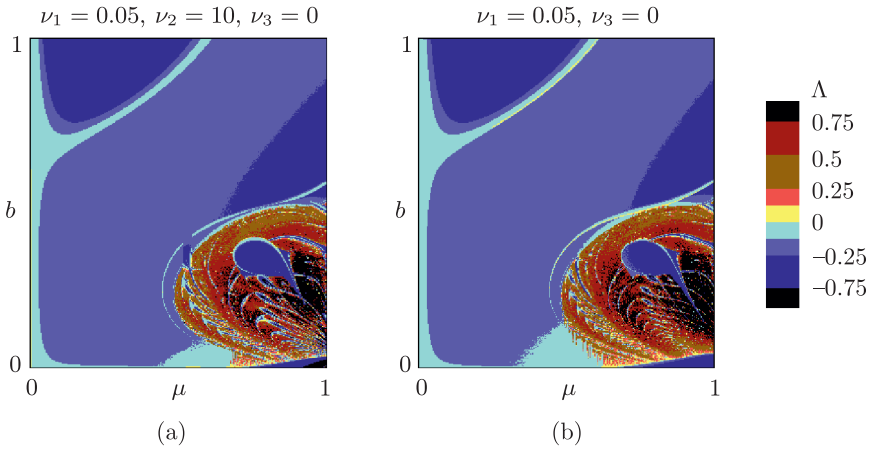


**Fig. 17.** Lyapunov charts for a system with small longitudinal and large transverse viscous friction (a) and for the nonholonomic model with longitudinal friction (b). The colors denote the value of the largest Lyapunov exponent in accordance with the legend on the right. The friction coefficients are given in the captions. The other parameters are $b = 1$, $a = 0.5$, $J_0 = 0.05$.

to that of a Chaplygin sleigh when the nonholonomic constraint prohibiting motions across the direction of the knife edge or skate placed on the platform is replaced by viscous friction.

Based on numerical simulations, we have made a comparison of the main dynamical phenomena for the nonholonomic model and for the system with friction.

It is shown that the effect of acceleration of motion of the platform under small oscillations of the internal mass, as observed in the nonholonomic model, persists when the nonholonomic constraint is replaced by transverse viscous friction in the region of small velocities, but, in contrast to the nonholonomic model, the increase in the velocity has the tendency to saturation.

The special features are shown of the transformation of fractal attractors, which occur in the space of generalized momenta of the nonholonomic model and are similar to those occurring in dissipative systems, and "fat" attractors, which are similar to the "chaotic sea" in Hamiltonian systems. It is demonstrated that, apart from some minor changes, the attractors of the first type persist when the nonholonomic constraint is replaced by viscous friction, and the attractors of the second type break down, resulting in the formation of many coexisting regular attractors in the form of attracting cycles. This is the most significant qualitative difference of the dynamical behavior of the nonholonomic model and the system with friction.

It is shown that, in the system with viscous friction, the motions in the laboratory reference frame which are associated with strange attractors and have the form of two-dimensional random walks persist, but are characterized by a smaller value of the diffusion coefficient as compared to the nonholonomic model.

In the nonholonomic model where longitudinal viscous friction is taken into account, the effect of parametric resonance can lead to an unbounded growth of the kinetic energy of the platform with unbounded excitation of the oscillation amplitude. In the system where the nonholonomic constraint is replaced by transverse viscous friction, the effect of parametric resonance is characterized by saturation of parametric instability. Also, the steady-state average velocity of motion of the platform in the laboratory reference system turns out to be bounded.

It is shown that in the parameter space of the nonholonomic model and of the system with viscous friction the arrangement of the regions of regular dynamics and chaotic dynamics is in both cases similar, as are the bifurcation scenarios leading to the onset of chaos.

## ACKNOWLEDGMENTS

The work of A. V. Borisov (Introduction and formulation of the equations of motion (Section 1)) was supported by the RFBR under grants No. 18-08-00999-a and 18-29-10051-mk. Numerical simulation and analysis of the results obtained (Sections 2–6) were carried out by A. V. Borisov and S. P. Kuznetsov within the framework of the RSF grant No. 15-12-20035.

## REFERENCES


1. Yuh, J., Design and Control of Autonomous Underwater Robots: A Survey, *Auton. Robots,* 2000, vol. 8, no. 1, pp. 7–24.
2. Whitcomb, L., Yoerger, D. R., Singh, H., and Howland, J., Advances in Underwater Robot Vehicles for Deep Ocean Exploration: Navigation, Control, and Survey Operations, in *Robotics Research,* J. M. Hollerbach, D. E. Koditschek (Eds.), London: Springer, 2000, pp. 439–448.
3. Karavaev, Yu. L., Kilin, A. A., and Klekovkin, A. V., Experimental Investigations of the Controlled Motion of a Screwless Underwater Robot, *Regul. Chaotic Dyn.,* 2016, vol. 21, nos. 7–8, pp. 918–926.
4. Andersen, A., Pesavento, U., and Wang, Z. J., Analysis of Transitions between Fluttering, Tumbling and Steady Descent of Falling Cards, *J. Fluid Mech.,* 2005, vol. 541, pp. 91–104.
5. Pesavento, U. and Wang, Z. J., Falling Paper: Navier – Stokes Solutions, Model of Fluid Forces, and Center of Mass Elevation, *Phys. Rev. Lett.,* 2004, vol. 93, no. 14, 144501, 4 pp.
6. Tanabe, Y. and Kaneko, K., Tanabe and Kaneko Reply, *Phys. Rev. Lett.,* 1995, vol. 75, no. 7, p. 1421.
7. Kozlov, V. V., On the Problem of Fall of a Rigid Body in a Resisting Medium, *Mosc. Univ. Mech. Bull.,* 1990, vol. 45, no. 1, pp. 30–36; see also: *Vestn. Mosk. Univ. Ser. 1. Mat. Mekh.,* 1990, no. 1, pp. 79–86.
8. Kuznetsov, S. P., Plate Falling in a Fluid: Regular and Chaotic Dynamics of Finite-Dimensional Models, *Regul. Chaotic Dyn.,* 2015, vol. 20, no. 3, pp. 345–382.
9. Borisov, A. V., Kuznetsov, S. P., Mamaev, I. S., and Tenenev, V. A., Describing the Motion of a Body with an Elliptical Cross Section in a Viscous Uncompressible Fluid by Model Equations Reconstructed from Data Processing, *Tech. Phys. Lett.,* 2016, vol. 42, no. 9, pp. 886–890; see also: *Pis'ma Zh. Tekh. Fiz.,* 2016, vol. 42, no. 17, pp. 9–19.
10. Chaplygin, S. A., On the Theory of Motion of Nonholonomic Systems. The Reducing-Multiplier Theorem, *Regul. Chaotic Dyn.,* 2008, vol. 13, no. 4, pp. 369–376; see also: *Mat. Sb.,* 1912, vol. 28, no. 2, pp. 303–314.
11. Carathéodory, C., Der Schlitten, *Z. Angew. Math. Mech.,* 1933, vol. 13, no. 2, pp. 71–76.
12. Borisov, A. V. and Mamaev, I. S., The Dynamics of a Chaplygin Sleigh, *J. Appl. Math. Mech.,* 2009, vol. 73, no. 2, pp. 156–161; see also: *Prikl. Mat. Mekh.,* 2009, vol. 73, no. 2, pp. 219–225.
13. Borisov, A. V. and Kuznetsov, S. P., Regular and Chaotic Motions of Chaplygin Sleigh under Periodic Pulsed Torque Impacts, *Regul. Chaotic Dyn.,* 2016, vol. 21, nos. 7–8, pp. 792–803.
14. Kuznetsov, S. P., Regular and Chaotic Motions of the Chaplygin Sleigh with Periodically Switched Location of Nonholonomic Constraint, *Europhys. Lett.,* 2017, vol. 118, no. 1, 10007, 10 pp.
15. Kuznetsov, S. P., Regular and Chaotic Dynamics of a Chaplygin Sleigh due to Periodic Switch of the Nonholonomic Constraint, *Regul. Chaotic Dyn.,* 2018, vol. 23, no. 2, pp. 178–192.
16. Bizyaev, I. A., Borisov, A. V., and Kuznetsov, S. P., Chaplygin Sleigh with Periodically Oscillating Internal Mass, *Europhys. Lett.,* 2017, vol. 119, no. 6, 60008, 7 pp.
17. Bizyaev, I. A., Borisov, A. V., and Mamaev, I. S., The Chaplygin Sleigh with Parametric Excitation: Chaotic Dynamics and Nonholonomic Acceleration, *Regul. Chaotic Dyn.,* 2017, vol. 22, no. 8, pp. 957–977.
18. Bizyaev, I. A., Borisov, A. V., and Kuznetsov, S. P., The Chaplygin Sleigh with Friction Moving due to Periodic Oscillations of an Internal Mass, *Nonlinear Dyn.,* 2018, 16 pp.
19. Tallapragada, Ph. and Fedonyuk, V., Steering a Chaplygin Sleigh Using Periodic Impulses, *J. Comput. Nonlinear Dynam.,* 2017, vol. 12, no. 5, 054501, 5 pp.
20. Fedonyuk, V. and Tallapragada, Ph., Stick-Slip Motion of the Chaplygin Sleigh with Piecewise-Smooth Nonholonomic Constraint, *ASME J. Comput. Nonlin. Dyn.,* 2017, vol. 12, no. 3, 031021, 8 pp.
21. Fedonyuk, V. and Tallapragada, Ph., Sinusoidal Control and Limit Cycle Analysis of the Dissipative Chaplygin Sleigh, *Nonlinear Dyn.,* 2018, vol. 93, no. 2, pp. 835–846.
22. Fermi, E., On the Origin of the Cosmic Radiation, *Phys. Rev.,* 1949, vol. 75, no. 8, pp. 1169–1174.
23. Zaslavsky, G. M. and Chirikov, B. V., Fermi Acceleration Mechanism in the One-Dimensional Case, *Dokl. Akad. Nauk SSSR,* 1964, vol. 159, no. 2, pp. 306–309 (Russian).
24. Zaslavskii, G. M. and Chirikov, B. V., Stochastic Instability of Non-Linear Oscillations, *Sov. Phys. Usp.,* 1972, vol. 14, no. 5, pp. 549–568; see also: *Uspekhi Fiz. Nauk,* 1971, vol. 105, no. 9, pp. 3–39.
25. Zaslavsky, G. M., *Statistical Irreversibility in Nonlinear Systems,* Moscow: Nauka, 1970 (Russian).
26. *Handbook of Chaos Control,* E. Schöll, H. G. Schuster (Eds.), 2nd ed., Weinheim: Wiley-VCH, 2008.
27. Karapetyan, A. V., On Realizing Nonholonomic Constraints by Viscous Friction Forces and Celtic Stones Stability, *J. Appl. Math. Mech.,* 1981, vol. 45, no. 1, pp. 30–36; see also: *Prikl. Mat. Mekh.,* 1981, vol. 45, no. 1, pp. 42–51.
28. Kozlov, V. V., On the Realization of Constraints in Dynamics, *J. Appl. Math. Mech.,* 1992, vol. 56, no. 4, pp. 594–600; see also: *Prikl. Mat. Mekh.,* 1992, vol. 56, no. 4, pp. 692–698.
29. Neimark, Ju. I. and Fufaev, N. A., *Dynamics of Nonholonomic Systems,* Trans. Math. Monogr., vol. 33, Providence, R.I.: AMS, 2004.
30. Fufaev, N. A., On the Possibility of Realizing a Nonholonomic Constraint by Means of Viscous Friction Forces, *J. Appl. Math. Mech.,* 1964, vol. 28, no. 3, pp. 630–632; see also: *Prikl. Mat. Mekh.,* 1964, vol. 28, no. 3, pp. 513–515.
31. Lamb, H., *Hydrodynamics,* 6th ed., Cambridge: Cambridge Univ. Press, 1993.

32. Ruelle, D., Strange Attractors, *Math. Intelligencer,* 1980, vol. 2, no. 3, pp. 126–137.
33. Schuster, H. G. and Just, W., *Deterministic Chaos: An Introduction,* Weinheim: Wiley-VCH, 2005.
34. Kuznetsov, S. P., *Dynamical Chaos,* 2nd ed., Moscow: Fizmatlit, 2006 (Russian).
35. Sagdeev, R. Z., Usikov, D. A., and Zaslavsky, G. M., *Nonlinear Physics: From the Pendulum to Turbulence and Chaos,* Chur: Harwood, 1990.
36. Lichtenberg, A. J. and Lieberman, M. A., *Regular and Chaotic Dynamics,* 2nd ed., Appl. Math. Sci., vol. 38, New York: Springer, 1992.
37. Reichl, L. E., *The Transition to Chaos: Conservative Classical Systems and Quantum Manifestations,* 2nd ed., New York: Springer, 2004.
38. Feller, W., *An Introduction to Probability Theory and Its Applications: Vol. 1,* 3rd ed., New York: Wiley, 1968.
39. Rytov, S. M., Kravtsov, Yu. A., and Tatarskii, V. I., *Principles of Statistical Radiophysics: 1. Elements of Random Process Theory,* Berlin: Springer, 1987.
40. Cox, D. R. and Miller, H. D., *The Theory of Stochastic Processes,* London: Methuen, 1970.
41. Rabinovich, M. I. and Trubetskov, D. I., *Oscillations and Waves in Linear and Nonlinear Systems,* Dordrecht: Kluver, 1989.
42. Damgov, V., *Nonlinear and Parametric Phenomena: Theory and Applications in Radiophysical and Mechanical Systems,* Singapore: World Sci., 2004.
43. Champneys, A., Dynamics of Parametric Excitation, in *Mathematics of Complexity and Dynamical Systems: Vols. 1–3,* New York: Springer, 2012, pp. 183–204.
44. Borisov, A. V. and Mamaev, I. S., Strange Attractors in Rattleback Dynamics, *Physics–Uspekhi,* 2003, vol. 46, no. 4, pp. 393–403; see also: *Uspekhi Fiz. Nauk,* 2003, vol. 173, no. 4, pp. 407–418.
45. Borisov, A. V., Jalnine, A. Yu., Kuznetsov, S. P., Sataev, I. R., and Sedova, J. V., Dynamical Phenomena Occurring due to Phase Volume Compression in Nonholonomic Model of the Rattleback, *Regul. Chaotic Dyn.,* 2012, vol. 17, no. 6, pp. 512–532.
46. Borisov, A. V., Kazakov, A. O., and Kuznetsov, S. P., Nonlinear Dynamics of the Rattleback: A Nonholonomic Model, *Physics–Uspekhi,* 2014, vol. 57, no. 5, pp. 453–460; see also: *Uspekhi Fiz. Nauk,* 2014, vol. 184, no. 5, pp. 493–500.
47. Kaplan, J. L. and Yorke, J. A., A Chaotic Behavior of Multi-Dimensional Differential Equations, in *Functional Differential Equations and Approximations of Fixed Points,* H.-O. Peitgen, H.-O. Walther (Eds.), Lecture Notes in Math., vol. 730, Berlin: Springer, 1979, pp. 204–227.
48. Benettin, G., Galgani, L., Giorgilli, A., and Strelcyn, J.-M., Lyapunov Characteristic Exponents for Smooth Dynamical Systems and for Hamiltonian Systems: A Method for Computing All of Them: P. 1: Theory, *Meccanica,* 1980, vol. 15, no. 1, pp. 9–20.
49. Vasil'eva, A. B. and Butusov, V. F., Asymptotic Methods in Singular Perturbation Theory, Moscow: Vysshaja Shkola, 1990 (Russian).
50. Riznichenko, G. Yu., *Lectures on Mathematical Models in Biology,* Izhevsk: R&C Dynamics, Institute of Computer Science, 2011 (Russian).
51. Cole, J. D., *Perturbation Methods in Applied Mathematics,* Waltham, Mass.: Blaisdell, 1968.
52. Brendelev, V. N., On the Realization of Constraints in Nonholonomic Mechanics, *J. Appl. Math. Mech.,* 1981, vol. 45, no. 3, pp. 351–355; see also: *Prikl. Mat. Mekh.,* 1981, vol. 45, no. 3, pp. 481–487.
53. Kozlov, V. V., Realization of Nonintegrable Constraints in Classical Mechanics, *Sov. Phys. Dokl.,* 1983, vol. 28, pp. 735–737; see also: *Dokl. Akad. Nauk SSSR,* 1983, vol. 272, no. 3, pp. 550–554.
54. Eldering, J., Realizing Nonholonomic Dynamics As Limit of Friction Forces, *Regul. Chaotic Dyn.,* 2016, vol. 21, no. 4, pp. 390–409.